NASA

Technical Memorandum 80277

An Algorithm for Retrieval of Ocean Surface and Atmospheric Parameters from the Observations of the Scanning Multichannel Microwave Radiometer (SMMR)

T. T. Wilheit and A. T. C. Chang

(NASA-TM-80277) AN ALGORITHM FOR RETRIEVAL OF OCEAN SURFACE AND ATMOSPHERIC PARAMETERS FROM THE OBSERVATIONS OF THE SCANNING MULTICHANNEL MICROWAVE RADIOMETER (SMMR) (NASA) 36 p HC A04/MF A01 CSCL 08C G3/43

N79-27635

Unclas 29954

MAY 1979

National Aeronautics and Space Administration

Goddard Space Flight Center
Greenbelt, Maryland 20771

TM 80277

AN ALGORITHM FOR RETRIEVAL OF OCEAN SURFACE AND ATMOSPHERIC PARAMETERS FROM THE OBSERVATIONS OF THE SCANNING MULTICHANNEL MICROWAVE RADIOMETER (SMMR)

T. T. Wilheit and A. T. C. Chang

May 1979

GODDARD SPACE FLIGHT CENTER
Greenbelt, Maryland 20771

AN ALGORITHM FOR RETRIEVAL OF OCEAN SURFACE AND ATMOSPHERIC PARAMETERS FROM THE OBSERVATIONS OF THE SCANNING MULTICHANNEL MICROWAVE RADIOMETER (SMMR)

T. T. Wilheit and A. T. C. Chang

NASA/Goddard Space Flight Center

ABSTRACT

The Scanning Multichannel Microwave Radiometer (SMMR) is a 5-frequency (6.6, 10.7, 18, 21, and 37 GHz dual polarized microwave radiometer which was launched in two separate satellites, Nimbus-7 and Seasat in 1978. A formalism is developed which can be used to interpret the data in terms of sea surface temperature, sea surface wind speed, and the atmospheric overburden of water vapor and liquid water. It is shown with reasonable instrumental performance assumptions, these parameters can be derived to useful accuracies. Although the algorithms are not derived for use in rain; it is shown that, at least, token rain rates can be tolerated without invalidating the retrieved geophysical parameters.

CONTENTS

TABLES

ILLUSTRATIONS

ILLUSTRATIONS (continued)

AN ALGORITHM FOR RETRIEVAL OF OCEAN SURFACE AND ATMOSPHERIC PARAMETERS FROM THE OBSERVATIONS OF THE SCANNING MULTICHANNEL MICROWAVE RADIOMETER (SMMR)

SECTION I

INTRODUCTION

The Scanning Multichannel Microwave Radiometer (SMMR) was carried aboard both the Nimbus-7 and Seasat satellites, both of which were launched in 1978. It is a 5 frequency, dual polarized microwave radiometer which scans an 80 cm reflector such that the antenna beam sweeps a conical arc of 50° with a cone angle of 42° measured at the spacecraft. This provides constant incidence angle of approximately 49° (for an 800 km orbit) at the Earth's surface when the cone axis is aligned with the local vertical (its nominal orientation). The primary purpose of this instrument is to measure the sea surface temperature, sea surface wind speed, and the atmospheric content of water vapor and liquid water (clouds) under nearly all weather conditions. It is the purpose of this paper to derive a formalism for extracting these parameters from the measurements provided by the SMMR. A similar derivation was provided by Chang and Wilheit (1979) for interpretation of a three channel system. We will refer to this paper for computational details and only repeat enough for conceptual self-sufficiency in this paper. We will also draw heavily on review articles by Wilheit (1978) and Wilheit et al. (1978) for background discussions.

In Section II, we will treat the relationships between the geophysical variables and the brightness temperatures. An approach for extracting the geophysical parameters from the brightness temperature will be developed in Section III and numbers will be calculated based on the models of Section II. In Section IV we will develop an algorithm for approximating rain intensity from the radiometer measurements. In Section V, we will examine the sensitivity of these algorithms to rain filling all or part of the field of view. In Appendix I we will give computer programs for all the retrievals and explanations of them.

SECTION II

BACKGROUND PHYSICS

Because of the validity of the Rayleigh Jeans approximation in the microwave region, the law of radiative transfer may be expressed quite simply

$$\frac{dT_B}{dx} = -\gamma (T_B - t_o) \tag{1}$$

where T_B is the microwave radiance expressed as an equivalent black body temperature, γ is the absorption coefficient at the point x and t_o is the thermodynamic temperature of the medium at that point.

The derivative is along the direction of propagation. It must be emphasized that γ is only the attenuation due to loss mechanisms; scattering and reflection must be accounted for by appropriate re-distribution of radiation among directions of propagation.

A typical Earth viewing geometry is shown in Figure 1. In order to calculate the brightness temperature expected for such a situation one first divides the atmosphere up into a number of layers each of which may be characterized by a uniform temperature and absorption coefficient. Beginning with the 3°K cosmic background, the radiation is then propagated from the top downwards through each layer according to Equation 1. A fraction R (the reflectivity) is reflected from the surface and the surface also radiates an amount Et where E is a quantity characteristic of the surface, the emissivity, having a value between 0 and 1 and t is the thermodynamic temperature of the surface. Arguments based on thermodynamic equilibrium show that E and R are related by:

$$E + R = 1 \tag{2}$$

Since water is a polar molecule it has a very large dielectric constant at microwave frequencies. This results in a large reflectivity (low emissivity) for a liquid water surface such as the ocean. In Figure 2, the emissivity, calculated for a smooth water surface using the dielectric constant data for 20°C of Lane and Saxton (1952) and the Fresnel relations (Jackson 1962), is shown. Note that the emissivity increases somewhat with frequency over the range, and that for viewing at an oblique angle, the horizontal polarization yields a lower and vertical a higher emissivity than that for nadir

viewing where the distinction between the two polarizations breaks down. The emissivity was calculated both for fresh water and for a 3.5% NaCl solution which is a reasonable approximation to sea water; there is no consequential difference between fresh and sea water except at the very low frequency end of the spectrum, below about 5 GHz. Since most solid surfaces have emissivities in the range 0.8 to 0.95 and 0.5 is a typical value for water, there is a striking contrast between liquid water surfaces such as lakes, rivers, and the oceans and solid surfaces such as land and sea ice. This low emissivity of the sea surface also provides a good background for viewing the intervening atmosphere.

The emissivities shown in Figure 2 were calculated for a smooth water surface. However, when the wind blows across the surface of the ocean, it generates roughness and foam. Some care is required in the quantitative definition of wind speed at the surface. There is a substantial vertical gradient in the wind speed in the boundary layer. A turbulent wind shear model for the marine boundary layer has been developed by Cardone (1969). In this model, the details of the wind shear depend on the wind speed and on the air/sea temperature difference. In general, there is more shear if the ocean is colder than the air (stable) than if the ocean is warmer than the air (unstable). Wherever possible wind speeds used in the derivation of the emissivity models defined as follows: The wind speed is measured at any altitude within the marine boundary layer. Using the actual air and sea temperatures, the friction velocity (generally termed "U-Star" (U*)) is calculated with the Cardone (1969) model. Then, assuming neutral stability (air/sea temperature equal), the wind speed at 20 m altitude is calculated. This last step is merely a translation of U* into a more familiar quantity. The results of Wilheit (1978 II) suggest that this is an appropriate definition. The effect of roughness on the emissivity of the water surface depends strongly on the viewing angle and polarization. For viewing directly at nadir where the distinction between vertical and horizontal polarizations disappears, roughness has very little effect on emissivity; for viewing in horizontal polarization at angles away from nadir, the roughness increases the emissivity and for vertical polarization for view angles between 0° (nadir) and 55° the roughness increases the emissivity while it decreases the emissivity for view angles greater than about 55°, as was determined experimentally by Hollinger (1971). Foam

cover, on the other hand, always increases the emissivity of the surface. Figure 3 shows the increase in brightness temperature caused by a given wind speed as found by Nordberg et al. (1971) for a frequency of 19.35 GHz and for nadir viewing. They found no effect, in their case, for wind speeds less than 7 m/s and an increase of around 1°Ks/m above that. This relationship has been investigated further by Webster et al. (1975). They examined a frequency range of from 1.4 to 37 GHz and a view angle of 38° (both polarizations). Figure 4 summarizes their results. Here the rate of increase of brightness temperature with increasing wind speed is shown for all frequencies observed. Note first that viewing in horizontal polarization enhances and viewing in vertical polarization decreases the strength of the effect vis-a-vis nadir viewing. This is because in horizontal polarization the effect of roughness and of foam both increase with increasing wind speed and because viewing in horizontal polarization decreases the emissivity of the undisturbed surface thereby increasing the emissivity contrast between the foam and open water with respect to nadir viewing. The converse argument for foam and the relative weakness of the roughness effect account for the vertical polarization case. Note also that the spectrum of the net effect is only weakly frequency dependent above about 10 GHz but it decreases somewhat at lower frequencies.

Wilheit (1978 II) has examined the roughness effect isolated from the atmosphere and foam effects both in satellite data (Nimbus-6 Electrically Scanned Microwave Radiometer) and in the data of Hollinger (1971).

It was found that the surface could be treated as an ensemble of flat surfaces and the emissivity calculated for each member of the ensemble as though it were an infinite plane surface. The rough surface emissivity is then the ensemble average of the individual emissivities. It was found that the distribution of surface slopes given by Cox and Munk (1954) overestimated the roughness effect below 35 GHz, but was acceptable at higher frequencies. In particular it was found that the variance of surface slopes σ^2 required to account for the microwave observations is given by:

$$\sigma^2 = (0.3 + 0.02\, f\,(\mathrm{GHz}))\, \sigma^2_{cm} \qquad f \leq 35\ \mathrm{GHz}$$

$$\sigma^2 = \sigma^2_{cm} \qquad f \geq 35\ \mathrm{GHz} \qquad (3)$$

where f is the observation frequency and σ^2_{cm} is the surface slope variance given by Cox and Munk (1955). A composite surface model which includes the effect of both roughness and foam was proposed by Wilheit (1979). In this model, the rough surface described is partially obscured by foam (for wind speeds greater than 7 m/s) such that R, the reflectivity of the surface, is reduced by:

$$R_{NET}(\theta, P) = (1 - K)\, R_{\substack{ROUGHNESS \\ ONLY}}(\theta, P)$$

$$K = a(1 - e^{-f/f_o})(w - 7\ m/s) \qquad w \geq 7\ m/s$$

$$K = 0 \qquad w \leq 7\ m/s \qquad (4)$$

where f is the observation frequency, w is the wind speed, θ the view angle, P the polarization and

$$a = 0.006\ S/m$$

$$f_o = 7.5\ GHz \qquad (5)$$

The constituents of the atmosphere which make consequential contributions to the brightness temperatures observed in this spectral region are molecular oxygen water vapor and water droplets. Molecular oxygen has a series of resonances in the 50-70 GHz region and a single isolated line at 119 GHz. The microwave properties of molecular oxygen in an atmospheric context have been discussed by Meeks and Lilly (1963) and by Carter et al. (1968). A very elegant model which accounts for the overlapping of the pressure broadened lines has been published by Rosenkrantz (1975). Since the mixing ratio of oxygen is substantially constant and the absorption coefficient is only very weakly temperature dependent, it contributes only a constant offset to surface observations is the 1-40 GHz region. It must be included in calculations using any of the above models but is simple enough that it will not be dealt with further here.

Water vapor has a fairly weak resonance at 22.2 GHz and very strong ones at 183 GHz and higher frequencies, the wings of which give significant contributions to the atmospheric opacity at all frequencies but particularly above about 10 GHz. The absorption coefficient for water vapor based on Staelin (1966) is given in Figure 5 for the 1962 U.S. standard atmosphere (AFCRL, 1965) for sea level and 8 km altitude. The absorption varies as a function of altitude because of pressure broadening. However, the bulk of water vapor is found in the bottom few kilometers of the atmosphere, over which there is little change in the pressure broadening. Thus, variations in the vertical distribution of water vapor cause little difficulty in retrieving surface parameters.

The absorption due to non-raining liquid water clouds is well described by the Rayleigh approximation (Gunn and East 1954) using the dielectric data of Lane and Saxton (1952). In Figure 6, we show the absorption coefficient for a cloud with a liquid water density of 1 gm/m^3 at three different temperatures (0°C, ±20°C). The absorption coefficient is almost precisely quadratic in frequency and varies by about a factor of three with temperature over the range shown. Since the spectrum is preserved with this temperature variation, the spectral characteristic may be used to correct for clouds even though the absolute amount of liquid water would be uncertain by a temperature dependent multiplicative factor. Additional discussion of the microwave properties of molecular oxygen, water vapor and clouds along with numerical expressions for calculating absorption coefficients can be found in Chang and Wilheit (1978).

Rain, on the other hand, provides a much more complicated situation. The particles are large enough compared to a wavelength that resonant effects occur and the absorption is no longer simply proportional to the net water content. Further, the spectrum of the absorption coefficient depends on the drop size distribution and scattering must be considered as well as absorption. A model for calculating the upwelling brightness temperature from a raining situation is discussed by Wilheit et al. (1977). At present, there is no adequate technique for correction of observations in the presence of rain. In Section IV we will develop an algorithm for determining rainfall intensity and in Section V we will approximate the rain intensity through which the retrieval of surface parameters may be performed within reasonable error limits.

SECTION III

RETRIEVAL OF GEOPHYSICAL PARAMETERS

Microwave instruments are typically limited in their spatial resolution by diffraction in the antenna aperture. Since in SMMR all frequencies share a common aperture, the spatial resolution with which it views the Earth's surface at a given frequency is proportional to the wavelength. The SMMR resolution varies from approximately 150 km at 6.6 GHz to 25 km at 37 GHz. If the various frequencies are to be used together to arrive at surface parameters, they must be reduced to a common basis so that all the measurements apply to the same area. One is, therefore, limited in the retrieval of any given parameter to the spatial resolution of the lowest frequency used. Since resolution is always to be desired, it is necessary to reduce the SMMR data to several bases at various resolutions. The present scheme which is indicated in Figure 7 is to reduce SMMR data to four grids. The first has a resolution of 150 km and has all five frequencies; it is used for surface temperature determination. The grid 2 has a resolution of 90 km and has all the frequencies except 6.6; it is used for wind speed retrievals. In principle, it is possible to use the sea surface temperature derived at grid 1 to arrive at an approximate sea surface temperature to use as an additional input parameter in grid 2 for refinement of the wind speed determination. The retrieval algorithm presently discussed does not make use of this but the structure exists in both the Nimbus and Seasat data processing schemes to do so; it remains a possible algorithm refinement to be used as confidence in the instrument and in the simpler retrievals grows. Grid 3 has a resolution of approximately 60 km at the three highest frequencies and is used for the atmospheric water retrievals. Both the wind speed and sea surface temperature can be used as additional input parameters in future algorithm versions. The fourth grid has only 37 GHz data, but at a resolution of 30 km. It is only used, in ocean applications, for providing structural information to the rain rate retrieval which depends primarily on the 18 GHz data. A paper by Njoku (1979) describes the very difficult process of reducing the SMMR outputs to these common bases.

As can be seen from the previous section, the brightness temperatures which would be observed upwelling from the atmosphere depend on many geophysical variables. Moreover, several of the

variables (temperature, humidity, and liquid water content) are, in themselves, continuous functions of height. Therefore, this problem has an infinite number of degrees of freedom. In the most general sense, a retrieval of geophysical variables from a finite set of observations could never be performed. We must resort to approximations and constrained solutions if we are to derive useful information.

One technique for retrieving geophysical parameters is the statistical technique which was applied, quite successfully, by Waters et al. (1975) to the problem of approximating the atmospheric temperature profile from microwave brightness temperature measurements in the molecular oxygen band ($\lambda \approx 5$ mm). In this technique, which is schematically represented in Figure 8, they begin with a statistical data base consisting of a large set of actual temperature soundings. For each of these soundings, they calculate the expected upwelling brightness temperature at all frequencies at which measurements are made. The temperatures at various heights are then regressed against the brightness temperature or functions of the brightness temperature to determine the most probable (if the statistics are Gaussian) temperature from each level.

If there is little information about a given level in the brightness temperatures, then the retrieved temperature will tend toward the a priori average of the statistical data set and the residual of the regression will not be much smaller than the variance of the a priori data set. It is to be noted that information about a given level can occur in a given measurement either directly through the equation of radiative transfer or indirectly through correlations inherent to the atmosphere itself.

This technique may be faulted in that any bias of the a priori data set is introduced into the retrieval. When the brightness temperatures are strongly related in a direct sense to the geophysical parameters being retrieved, this would be of little consequence, but where the coupling is through statistical correlations among the geophysical observables or when the retrieval offers only marginal improvement over the a priori statistics and the retrieved values will tend strongly toward the commonplace situations. When tested on actual data, this may well give average statistics which suggest a very good retrieval technique yet give poor results in the extraordinary situation which is often of the most interest. We, therefore, have modified this technique somewhat. We generate an artificial

data set subtending the approximate expected range in all the geophysical variables at issue and force any correlations among them to be zero or at least much smaller than expected in nature. As a by-product, this relieves us the necessity of providing a true statistical data base for combinations of parameters which have been measured sparsely or not at all. For each member of this ensemble, we calculate the ten brightness temperatures (5 frequencies, 2 polarizations) as well as the geophysical parameters of interest here, sea surface temperature, sea surface wind speed, the column densities of water vapor and cloud liquid water and a correction for refraction by atmospheric water vapor calculated according to Bean and Dutton (1966) which is used in interpreting the data from the Seasat altimeter.

Although the retrieval problem contains, in principle, an infinite number of degrees of freedom, there are four principal degrees of freedom here, sea surface temperature, sea surface wind speed and the net atmospheric content of cloud liquid water and water vapor. One would not expect details of the temperature profile of the atmosphere nor the vertical distribution of the two phases of atmospheric water to have a large effect. In fact, the specific frequency choice for the 21 GHz channel being a little off the water vapor resonance at 22.235 GHz was made, based on unpublished calculations by the authors, in order to reduce the minor dependence on the vertical distribution of water vapor to negligible proportions. Similar calculations by Westwater (1978) arrived at a similar conclusion.

The quasi-statistical data base used here consists of 90 surface models (10 wind speeds and 9 sea surface temperatures – see Table I) and 81 atmospheric models made by combining the 9 handbook atmospheric temperature profiles in Table II (AFCRL 1965) with the 9 cloud models listed in Table III. These cloud models were simply invented for the present purpose. Observations of cloud liquid water content are almost non-existent. These were chosen to give a wide range in the net liquid water content and vertical distribution of water. The observations of Wilheit and Fowler (1977) would suggest that these models are, at least, reasonable. The combination of all 90 surface models with all 81 atmospheric models provides a net data set with 7290 composite models. In addition to the brightness temperatures and geophysical parameters another variable must be

considered. Real spacecraft do not always fly in their nominal attitude but may depart from it by several degrees in pitch, roll, and/or yaw. Thus the angle at which the sensor views the Earth's surface can vary as a function of time and scan position. This effect is included in the calculations by alternately using 48° and 50° as the view angle as the computation steps through the 81 different atmospheres. The view angle is then treated as an additional observable and is included in the regression like an additional brightness temperature.

These models subtend the approximate range expected for each of the parameters but the expected correlations are left out. Even so absurd a combination as an arctic winter atmosphere over an ocean with a temperature is 299°K is included. This would tend to make simulated retrieval results somewhat pessimistic. A weak correlation is introduced between cloud liquid water and water vapor content in two ways. First, wherever a cloud introduced, the relative humidity is increased to 100% (with respect to the liquid phase). This introduces some variability in the vertical distribution of water vapor over that given by the handbook atmospheres which are generally rather smooth. The second effect included is spontaneous nucleation (Mason 1971). Liquid water droplets in clouds cannot be super-cooled lower than –40°C without freezing. Since ice clouds are transparent at these frequencies, the cloud liquid water content is set to zero for any level at which the temperature is less than 233°K. This reduces the liquid water content for the colder, and thus drier, atmospheres.

The regression technique is inherently linear but the problem at hand has some mild nonlinearities. The present algorithm uses two techniques for mitigating the effect of those nonlinearities. The first has already been alluded to, the use of functions of brightness temperature rather than the brightness temperatures themselves. One is free to choose any function of brightness temperature for use in the regression; the appropriateness of any particular choice is determined by the residuals of the regression analyses. On the basis of heuristic arguments by Wilheit et al. (1977) we have chosen to use the function:

$$F(T_B) \equiv \ln(280^\circ K - T_B)$$

in lieu of brightness temperature for the channels most affected by the atmospheric constituents, 18, 21, and 37 GHz.

The second approach for dealing with non-linearities is to iterate the solution. The application of iterative solutions in the present context is illustrated in Figure 9. A set of retrieval matrices are made using the entire ensemble and also various restricted subsets of the ensemble of geophysical models. The data are first interpreted using the retrieval based on the entire ensemble and the approximate values for the geophysical parameters are then used to select the matrix derived from the most appropriate restricted ensemble. In principle, one could procede to even more and more restricted ensembles. In the present algorithm, the application of this iteration is limited. The nonlinearity to be addressed is the onset of foam generation at wind speeds of 7 m/s. This produces an abrupt change in the slope of brightness temperature versus wind speed. The solution for the sea surface parameters (temperature and wind speed) are significantly affected by this abrupt change. Thus in both cases the solution is iterated once to decide whether the wind speed is above or below 7 m/s. The solution for atmospheric parameters is not particularly improved by such an iteration and so the atmospheric retrievals are not iterated. It was also found that the use of the 37 GHz channel only aided significantly in the case of cloud liquid water. So, to aid in the isolation of possible problems with real data, it was not used in any of the other retrievals.

The assumed noise values were based on performance measurements of the engineering model of the SMMR instrument and approximations for the effect of averaging over the various grids. As a matter of judgement, no noise values less than 0.2°K were assumed. The values used are 0.2°K for the grid 1 and 2 retrievals and 0.5°K for the grid 3 retrievals. The assumed uncertainty in the incidence angle is 0.2° of angle. The resulting equations for the retrieval are as follows:

Wind Speed Retrieval – Wind Speed Unknown

$$\begin{aligned} WS\ (m/s) = &-465.3 + .6216\, T_{B10.7\,V} \\ &+ .2873\, T_{B10.7\,H} + 168.7 \ln (280. - T_{B18\,V}) \\ &- 86.31 \ln (280. - T_{B18\,H}) \\ &- 15.84 \ln (280. - T_{B21\,V}) \\ &- 37.18 \ln (280. - T_{B21\,H}) \\ &+ 2.357\, \theta_{INC} ; (1.8\,m/s / 12\,m/s) \end{aligned} \qquad (6)$$

Wind Speed < 7 m/s

$$\begin{aligned} WS\ (m/s) = & -523.9 - .2229\ T_{B10.7V} \\ & + .6056\ T_{B10.7H} + 130.3 \ln (280. - T_{B18V}) \\ & -39.19 \ln (280. - T_{B18H}) \\ & + 10.24 \ln (280. - T_{B21V}) \\ & -32.75 \ln (280. - T_{B21H}) \\ & +2.999\ \theta_{INC} : (1.6\ m/s / 1.9\ m/s) \end{aligned} \tag{7}$$

Wind Speed > 7 m/s

$$\begin{aligned} WS\ (m/s) = & -338.4 + .3115\ T_{B10.7V} \\ & + .4509\ T_{B10.7H} + 151.8 \ln (280. - T_{B18V}) \\ & - 91.12 \ln (280. - T_{B18H}) - 26.66 \ln (280. - T_{B21V}) \\ & + 12.89 \ln (280. - T_{B21H}) + 1.432\ \theta_{INC}, (1.0\ m/s / 10.0 m/s) \end{aligned} \tag{8}$$

Sea Surface Temperature (WS < 7 m/s)

$$\begin{aligned} SST\ (^{\circ}K) = & -149.1 + 1.677\ T_{B6.6V} + 1.666\ T_{B6.6H} \\ & - .2767\ T_{B10.7V} - .5590\ T_{B10.7H} \\ & + 46.17 \ln (280 - T_{B18V}) + 3.097 \ln (280. - T_{B18H}) \\ & .9162 \ln (280. - T_{B21V}) - 12.54 \ln (280. - T_{B21H}) \\ & - .5850\ \theta_{INC}\ (0.7^{\circ}C / 8.6^{\circ}C) \end{aligned} \tag{9}$$

Sea Surface Temperature (WS > 7 m/s)

$$\begin{aligned} SST\ (^{\circ}K) = & 188.9 + 3.040\ T_{B6.6V} - 1.188\ T_{B6.6H} \\ & - .709\ T_{B10.7V} + .2405\ T_{B10.7H} \\ & - 6.114 \ln (280. - T_{B18V}) + 20.37 \ln (280. - T_{B18H}) \\ & - 4.003 \ln (280. - T_{B21V}) + .986 \ln (280. - T_{B21H}) \\ & - 4.735\ \theta_{INC} : (1.5^{\circ}C / 8.6^{\circ}C) \end{aligned}$$

Cloud Liquid Water

$$\text{CLW}\ (\text{mg/cm}^2) = 246.1 - 51.72 \ln (280. - T_{B18V})$$
$$+ 134.4 \ln (280. - T_{B18H}) + 46.14 \ln (280. - T_{B21V})$$
$$+ 24.95 \ln (280. - T_{B21H}) - 155.5 \ln (280. - T_{B37V})$$
$$-36.63 \ln (280. - T_{B37H}) - 3.391\ \theta_{INC}\ ;\ (4.5\ \text{mg/cm}^2\ /\ 23\ \text{mg/cm}^2) \qquad (11)$$

Water Vapor

$$\text{WV}\ (\text{gm/cm}^2) = -9.784$$
$$+ 6.927 \ln (280. - T_{B18V}) + 5.361 \ln (280. - T_{B18H})$$
$$- 4.518 \ln (280. - T_{B21V}) - 6.081 \ln (280. - T_{B21H})$$
$$+ .039\ \theta_{INC}\ (.15\ \text{gm/cm}^2\ /\ 1.7\ \text{gm/cm}^2) \qquad (12)$$

Altimeter Wet Correction

$$\text{PL}\ (\text{cm}) = -51.95 + 34.37 \ln (280. - T_{B18V})$$
$$+ 37.15 \ln (280. - T_{B18H}) - 22.64 \ln (280. - T_{B21V})$$
$$- 39.70 \ln (280. - T_{B21H}) - .18\ \theta_{INC}\ ;\ (.9\ \text{cm}/10\ \text{cm}) \qquad (13)$$

The numbers in parenthesis following each equation represent respectively the RMS residual error of the regression and the RMS variability of the parameter in the original data set. Fortran IV programs which execute these equations and iterations are given in Appendix I.

SECTION IV

RAIN ALGORITHM

A model for quantitatively relating microwave brightness temperature to rain rate over ocean area was developed by Wilheit et al. (1977). In their model, the rain is treated as a Marshall-Palmer (1948) distribution of water droplets extending from the surface to the freezing level (0°C isotherm) with appropriate water vapor and non-raining cloud distributions. It is assumed that the water above the freezing level is frozen and thus essentially invisible to the frequencies of interest here. The full Mie (1908) scattering and absorption properties of the ensemble of droplets are calculated and the equation of radiative transfer solved with iteration to account for scattering. The problem is dominated by the microwave absorption by the rain with the scattering providing small corrections.

There are two major problems in the application of this model to the interpretation of measurements. The first is spatial resolution. The relationship between brightness temperature and rain rate which results from this model is highly non-linear. Thus if the rain intensity varies over the radiometer's instantaneous field of view, the brightness temperature which the antenna averages over the field of view in a linear manner will not yield an average rain rate but, in general, a lesser rain rate. At the 25 km resolution of the Nimbus-5 Electrically Scanned Microwave Radiometer (ESMR), this problem is serious; at the 60 km resolution of the 18 GHz channels of SMMR, the problem will be much worse. The 37 GHz channels have a resolution of 30 km but at rain rates on the order of 4 mm/hr or greater, the atmosphere is too opaque to yield useful rain intensity estimates. This represents too low a dynamic range to be useful. The 18 GHz can measure rain rates up to about 20 mm/hr, a much more reasonable dynamic range.

The second problem is that knowledge of the freezing level is required. Rao et al. (1977), in producing an atlas of oceanic rainfall from the Nimbus-5 ESMR data, used climatology to provide to the nearest 1 km a freezing level based on location and season. Since the freezing level was given in 1 km increments, changes in the freezing level produced abrupt changes in rain rates. A more serious problem was found at high altitudes where the climatological freezing levels were low (1 – 2 km). It was found that these low freezing levels caused the rainfall determinations to be clearly excessive.

As an ad hoc solution. The freezing level was set to 3 km for these cases. Since the maximum value for freezing level is about 5 km it was decided that the error contribution would not be too severe if the assumed freezing level were fixed at 4 km for the present. This can cause errors of ca. 25% in retrieved rain rate; the resolution problem can cause larger errors. The primary purpose of this rain algorithm is to flag the retrievals when the rain rate is excessive rather than to provide rain data per se. The effect of the rain on any channel depends first on the net opacity of the rain column at that frequency so fixing the freezing level should not have too great an effect on rain rates derived for this purpose. A more sophisticated rain retrieval should be used to derive rain data for climatological use.

In the present algorithm, we use the brightness at 18 GHz (horizontal polarization) for the primary rain information and 37 GHz to provide some help when the rain does not fill a grid 3 cell uniformly and to enhance the sensitivity to low rain rates. The brightness temperatures as a function of rain rate calculated by the Wilheit et al. (1977) model are given in Figure 10. The cell structures were arranged such that for each grid 3 cell there are four coincident grid 4 cells. The algorithm uses as input the 18H brightness temperature at grid 3 and for four corresponding (grid 4) 37H brightness temperatures. Three different cases may be defined.

1. All four 37H brightness temperatures saturated (rain rate $\gtrsim$ 4 mm/hr).

In this case the rain rate is derived from the 18H brightness only using a table corresponding to Figure 10.

2. All four 37H brightness yield meaningful rain rates (rain rates $\lesssim$ 4 mm/hr).

All 5 input values are converted to rain rates using the tabulated values and the results are averaged.

3. Some, but not all, of the 37 GHz brightness yield meaningful rain rates.

The meaningful rain rates for each of the grid 4 cells are converted to 18H brightness temperatures using tabulated values. Knowing these values and the average 18H brightness for all four grid 4 cells (i.e., the grid 3 measurement) an 18 GHz brightness temperature and thus rain rate can be calculated for the total area of the saturated 37 GHz measurements and the net rain rate for the whole grid 3 cell is calculated by appropriate averaging. A Fortran IV Program which executes this calculation is included in Appendix I.

SECTION V

SIMULATIONS TO DETERMINE THE RAIN SENSITIVITY OF THE GEOPHYSICAL ALGORITHMS

In order to test these algorithms for this sensitivity to rain, brightness temperatures were calculated according to the Wilheit et al. (1977) model for various rain rates and a few different surface conditions. These brightness temperatures were then averaged with brightness temperatures for no rain with various weights to simulate rain covering various percentages of the field of view. In Figure 11, we show the retrieved sea surface temperature as a function of rain rate averaged over the field of view for rain covering 1, 3, 10, 30, and 100% of the field of view. Figures 12 and 13 are similar representations of wind speed and water vapor retrievals. It can be seen that the retrieval errors induced by rain become comparable to the net retrieval error due to all other causes, and thus unacceptably large, in the neighborhood of 1.0, 0.75 and 0.5 mm/hr for sea surface temperature, sea surface wind speed and atmospheric water vapor content respectively. This is somewhat better performance than was reported by Wilheit et al. (1978). The algorithms were re-formulated, leaving out the 37 GHz channels, specifically to mitigate this rain sensitivity.

This sensitivity to rain may be understood by considering two situations. If there is a nominal rain rate, say 1 mm/hr, which covers the field of view uniformly the rain's contribution to the brightness temperature will be quite similar spectrally to that of non-raining clouds although much larger in magnitude. Thus, the retrieval algorithm for all parameters other than cloud liquid water will be only weakly affected. If, on the other hand there is a rain rate of 100 mm/hr covering 1% of the field of view, although the average rain rate is the same, the situation is altogether different. The rain column would be nearly opaque at all frequencies and would contribute similar brightness temperature increases at all frequencies when averaged over the field of view. This apparent spectrum is not similar to any in the data base from which the retrievals were derived and thus is not rejected and can affect the retrieval of any parameter. Other rain rates and spatial distributions can provide a wide range of apparent spectra. The strong dependence on the spatial distribution within the field of view suggests great difficulty in correcting for the rain.

This is not by any means a definitive calculation. We have ignored more complicated variations in the rain rate over the field of view and any effect the splashing of the rain drops may have on the surface emissivity. A more meaningful limit can be defined by comparing the errors between surface truth and retrievals from actual radiometric data with apparent rain rates also derived from actual spacecraft data.

SECTION VI

CONCLUSIONS

An algorithm has been derived for the retrieval of sea surface temperature, sea surface wind speed and the atmospheric overburden of water in the liquid and vapor phases. A refraction correction for the altimeter has also been derived. The achievable accuracies appear to be quite useful. For wind speeds greater than 7 m/s the wind speed precision appear to be about 1 meter/second and the sea surface temperature retrieval precision appear to be about 1.5°C. For low wind speeds ($\leq$ 7 m/s) the wind speed retrieval degrades to 1.6 m/s which is not much improvement over simply knowing that the wind speed is less than 7 m/s and the sea surface temperature retrieval improves to less than 1°C.

At any wind speed, the water vapor content of the atmosphere can be retrieved to a precision of 0.15 gm/cm^2 wet path length contribution to less than 1 cm and liquid water content to about 4 mg/cm^2.

REFERENCES

1. Air Force Cambridge Research Laboratory, Handbook of Geophysics and Space Environments, McGraw Hill, New York, 1965.
2. Bean, B. R., and E. J. Dutton, "Radio Meteorology," National Bureau of Standards Monograph #92 (1966).
3. Carter, C. J., R. L. Mitchell, and E. E. Reber, "Oxygen Absorption Measurements in the Lower Atmosphere," J. Geophys. Res. *73*, 3113-3120 (1968).
4. Cardone, V. J., "Specification of the Wind Distribution in the Marine Boundary Layer for Wave Forecasting," Ph.D. Thesis, New York University, Department of Meteorology and Oceanography, 1969 (Available from NTIS Order #AD702490).
5. Chang, A. T. C., and T. Wilheit, "Remote Sensing of Atmospheric Water Vapor, Liquid Water, and Wind Speed at the Ocean Surface by Passive Microwave Techniques from the Nimbus-5 Satellite," To be published in Radio Science (1979).
6. Cox, C. and Munk, W., Some Problems in Optical Oceanography, J. Marine Res. *14*, 63-78 (1955).
7. Gunn, L. L. S., and T. U. R. East, "The Microwave Properties of Precipitation Particles," Quart. J. Roy. Meteorol. Soc. 80, 522-554 (1954).
8. Hollinger, J. P., "Passive Microwave Measurements of Sea Surface Roughness," Trans. IEEE Geoscience Electronics, GE-9, pp 165-169 (1971).
9. Jackson, J. D., "Classical Electrodynamics," John Wiley & Sons, Inc., New York (1962), p 216ff.
10. Lane, J. A., and J. A. Saxton, "Dielectric Dispersion in Pure Polar Liquids at Very High Radio Frequencies," Proc. Roy. Soc., London A, 214, pp 531-545 (1952).
11. Marshall, T. S., and W. McK. Palmer, "The Distribution of Raindrops with Size," *J. Meteor.*, 5, 165-166 (1948).
12. Mason, J., "The Physics of Clouds," Clarendon Press, Oxford (1971).

13. Meeks, M. L., and A. E. Lilley, "The Microwave Spectrum of Oxygen in the Earth's Atmosphere," J. Geophys. Res., *68*, 1683-1703 (1963).

14. Mie, G., 1908: Beiträge zur Optik trüber Medien, speziell kolloidaler Metallösungen. *Ann Phys., 26,* 597-614.

15. Njoku, E. G., "Antenna Pattern Correction Procedures for the Scanning Multichannel Microwave Radiometer (SMMR)," To be published in Bdy. Layer Met. (1979).

16. Nordberg, W., J. Conaway, D. B. Ross, and T. Wilheit, "Measurements of Microwave Emission from a Foam-Covered Wind Driven Sea," J. Atmos. Sci., 38, 429-435 (1971).

17. Rao, M. S. V., W. V. Abbott, III, and J. S. Theon, "Satellite Derived Global Oceanic Rainfall Atlas (1973 and 1974)," NASA-X-911-76-116, June 1976.

18. Rosenkrantz, P. W., "Shape of the 5 MM Oxygen Band in the Atmosphere," Trans. IEEE (AP) (AP-23) 498-506 (1975).

19. Staelin, D. A., "Measurements and Interpretation of the Microwave Spectrum of the Terrestrial Atmosphere Near 1 Centimeter Wavelength," J. Geophys. Res., *71,* 2875-2881, 1966.

20. Waters, J. W., K. F. Kunzi, R. L. Pettyjohn, R. K. L. Poon, and D. H. Staelin, Remote Sensing of Atmospheric Temperature Profiles with Nimbus-5 Microwave Spectrometer, JAS, Vol. *32,* pp 1953-1969, 1975.

21. Webster, W. J., Jr., T. T. Wilheit, D. B. Ross, and P. Gloersen, "Spectral Characteristics of the Microwave Emission from a Wind Driven Foam-Covered Sea," J. Geophys. Res. *81,* 3095-3099 (1976).

22. Westwater, E. R., "The Accuracy of Water Vapor and Cloud Liquid Determination by Dual-Frequency Ground-Based Microwave Radiometry," Radio Science *13,* 677-685 (1978).

23. Wilheit, T. T., A. T. C. Chang, M. S. V. Rao, E. B. Rodgers, and J. S. Theon, "A Satellite Technique for Quantitatively Mapping Rainfall Rates Over the Oceans," J. Appl. Meteor., *16,* 551-650 (1977).

24. Wilheit, T. T., "A Review of Applications of Microwave Radiometry to Oceanography," Bdy. Layer Met. *13,* 277-293 (1978) I.

25. Wilheit, T. T., "The Effect of Wind on the Microwave Emission from the Ocean's Surface at 37 GHz," NASA TM-79588, July 1978 II, to be published in J. Geophys. Res.

26. Wilheit, T. T., "Atmospheric Corrections to Passive Microwave Observations of the Ocean," Invited Paper Presented at the Inter. Union Commission on Radio Meteorology Colloquium on Passive Radiometry of the Ocean's Surface," Patricia Bay, B. C., Canada, 1978, to be published in Bdy. Layer Met.

27. Wilheit, T. T., "A Model for the Microwave Emissivity of the Ocean's Surface as a Function of Wind Speed," NASA TM 80278, April 1979, Submitted to Trans. IEEE (GE).

Table I

Surface Models

Wind Speeds (m/s)		Sea Surface Temperatures (°K)
	1.	271
	2.	276.
Low Wind	4.	280.
	6.	283.
	8.	286.
	12.	289.
	17. High Wind	292.
	23.	295.
	30.	299.
	38.	

Tab'e II

Model Atmospheres

Name	Integrated Water Vapor
1. U.S. Standard	1.60 - 2.87 cm
2. Tropical	3.88 - 6.70
3. Subtropical Summer	4.23 - 6.95
4. Subtropical Winter	2.12 - 3.71
5. Mid-Latitude Summer	2.93 - 5.22
6. Mid-Latitude Winter	0.87 - 1.40
7. Subarctic Summer	2.07 - 3.11
8. Subarctic Winter (Cold)	0.43 - 0.64
9. Arctic Winter (Cold)	0.21 - 0.32

NOTE: Relative humidity set to 100% wherever cloud liquid density is greater than zero.

Table III

Cloud Models

Bottom (km)	Top (km)	Density (gm/m^3)	Max. Liquid Water (mg/cm^2)
1	2	0.1	10
1	2	0.3	30
0	8	0.1	80
7	8	0.2	20
1	3	0.04	8
1	3	0.08	16
2	4	0.02	4
6	8	0.2	40
-	-	0	0

NOTE: Density set to zero where atmospheric temperature $<40^{\circ}C$ (limit of supercooled water).

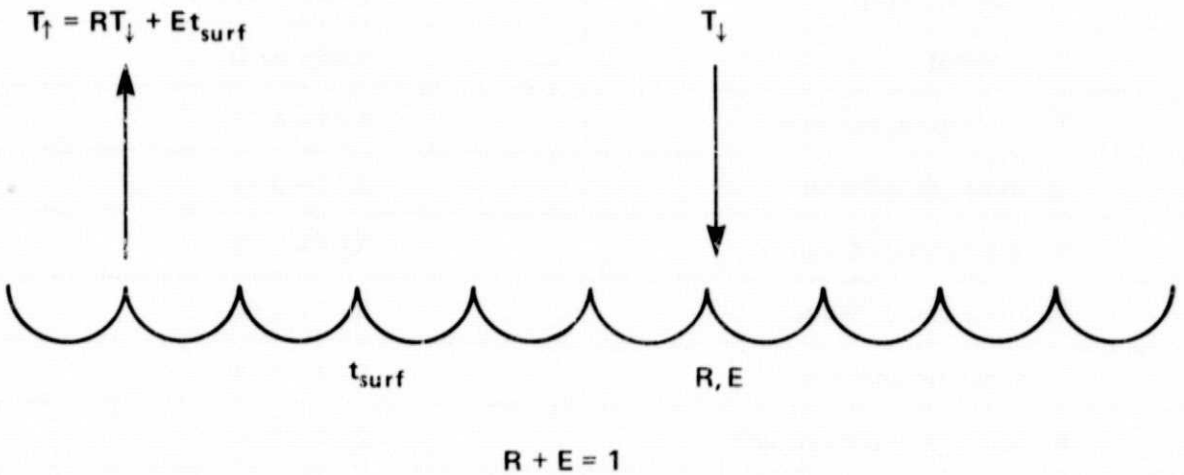

Figure 1. Typical Earth Viewing Geometry Showing the Effect of Reflection of a Microwave Radiance Expressed as a Brightness Temperature Off a Surface such as the Ocean where $T_{\downarrow}$ is the Downwelling Brightness Temperature, $T_{\uparrow}$ the Upwelling Brightness Temperature and E, R and t_{surf} the Emissivity, Reflectivity and Thermodynamic Temperature of the Surface Respectively

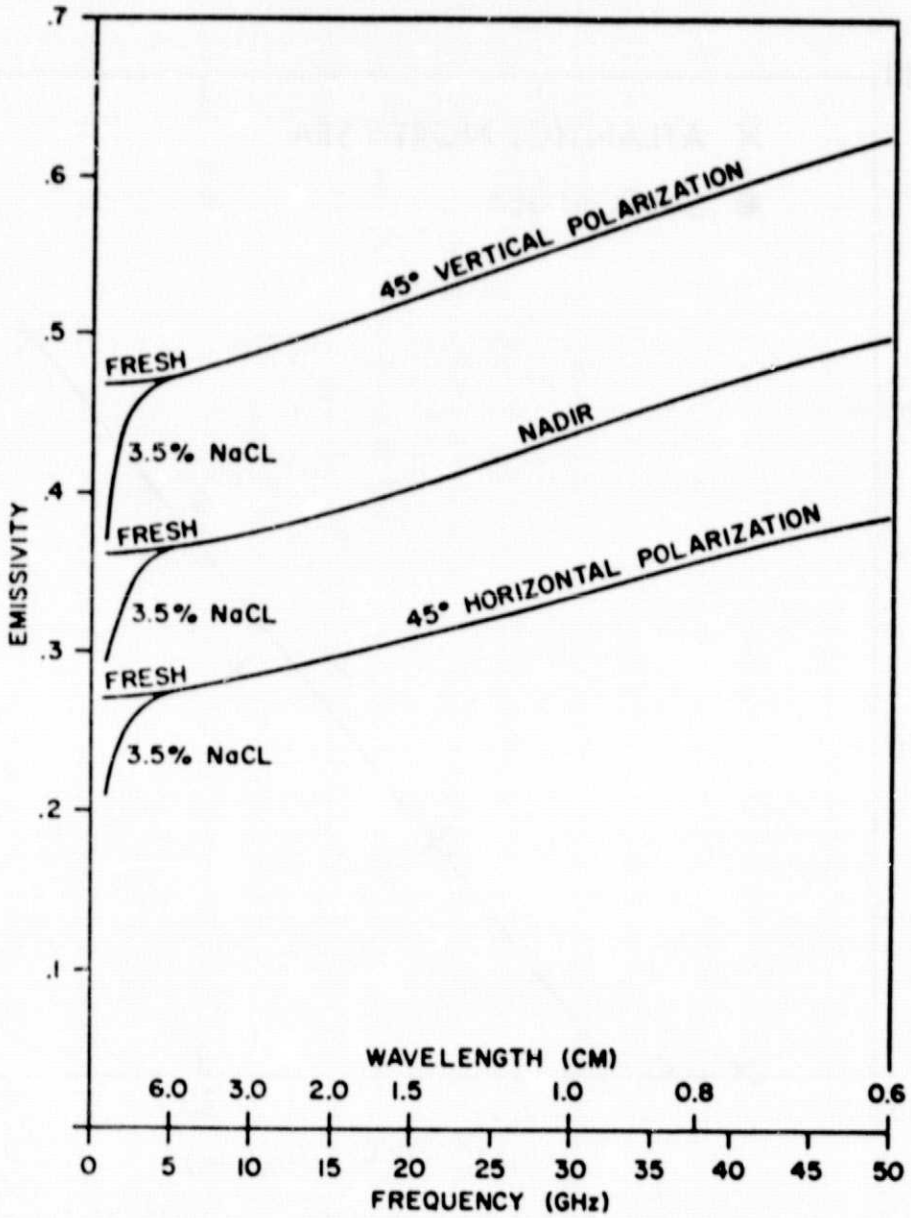

Figure 2. Emissivity of a Smooth Water Surface at 20°C

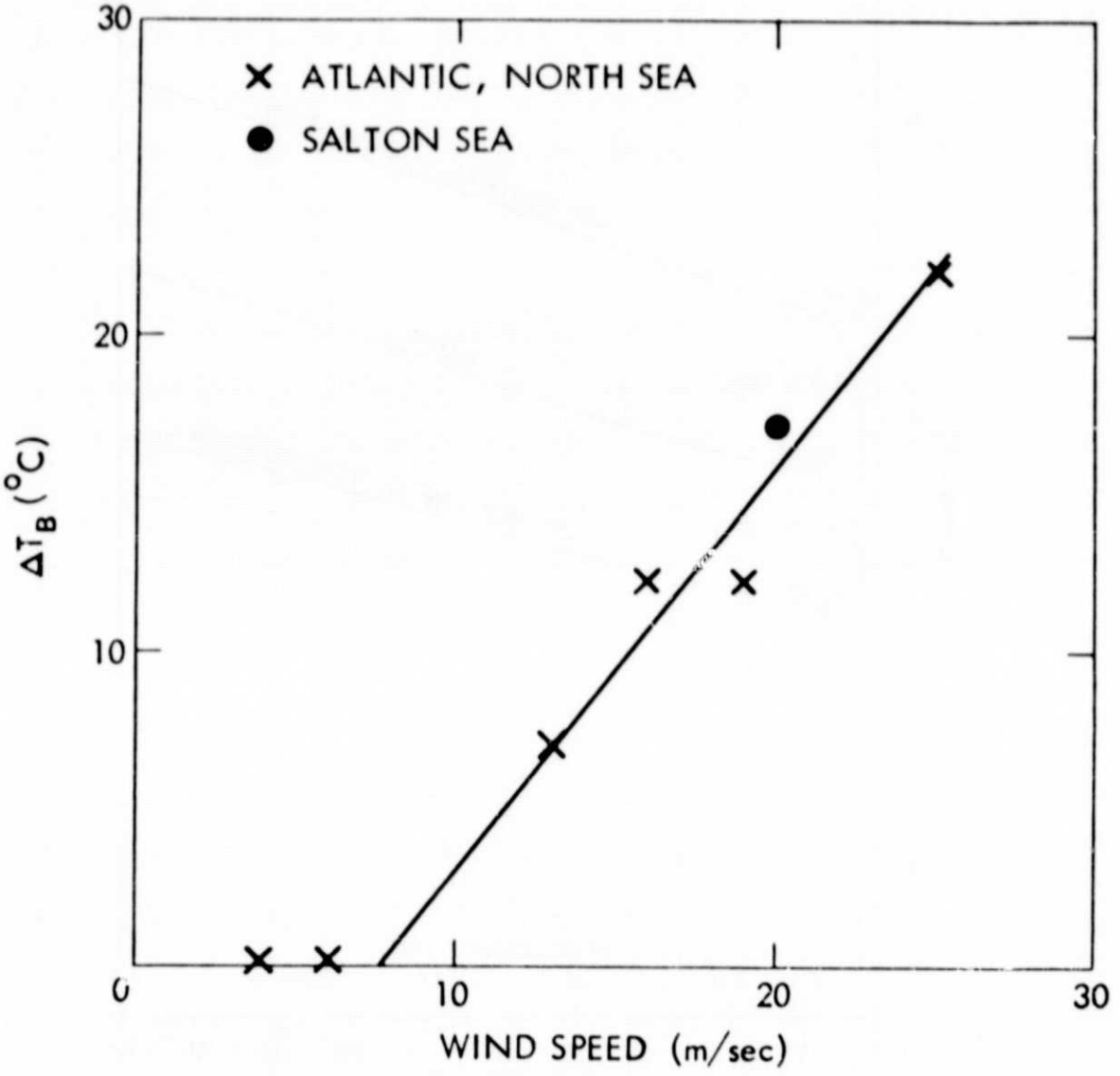

Figure 3. Increase in Brightness of the Ocean Surface (Et_{surf}) at 19.35 GHz Due to Wind Speed (Nordberg et al. (1971))

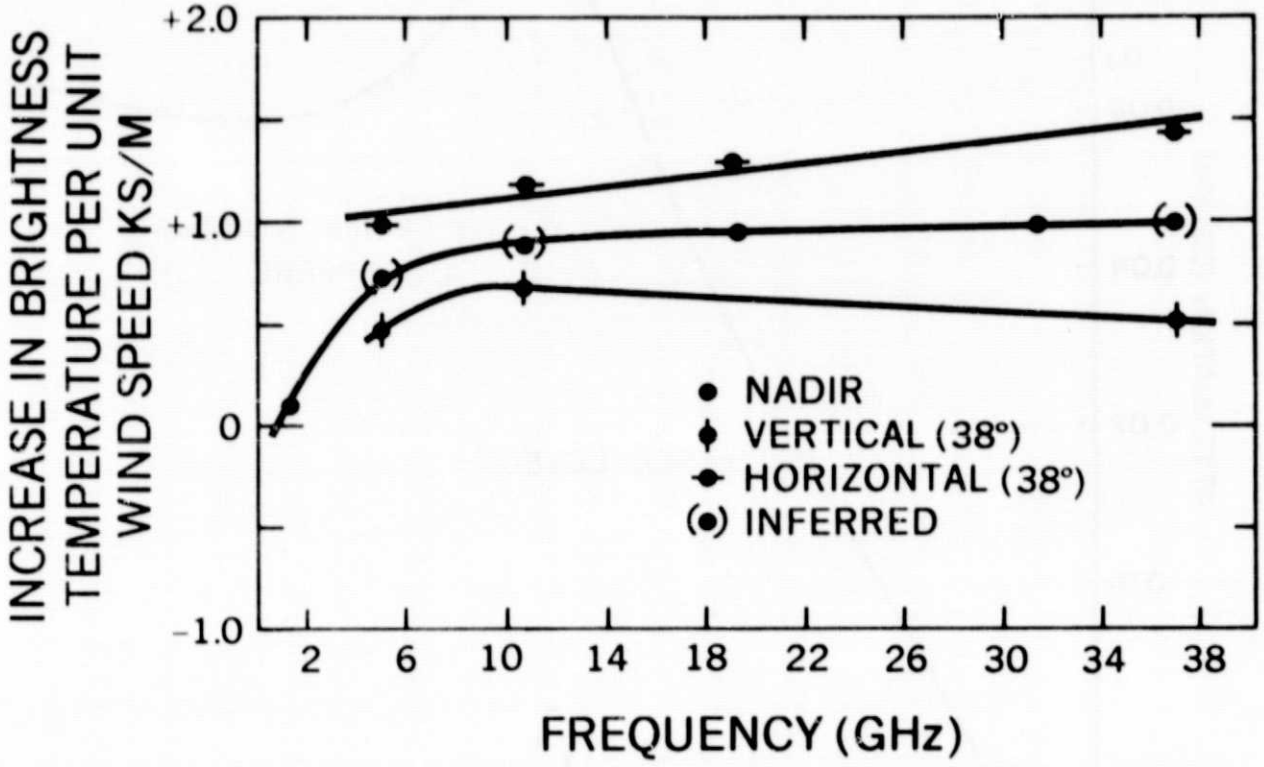

Figure 4. Spectrum of Increase in Brightness Temperature Caused by Wind at the Ocean Surface (Webster et al. (1975))

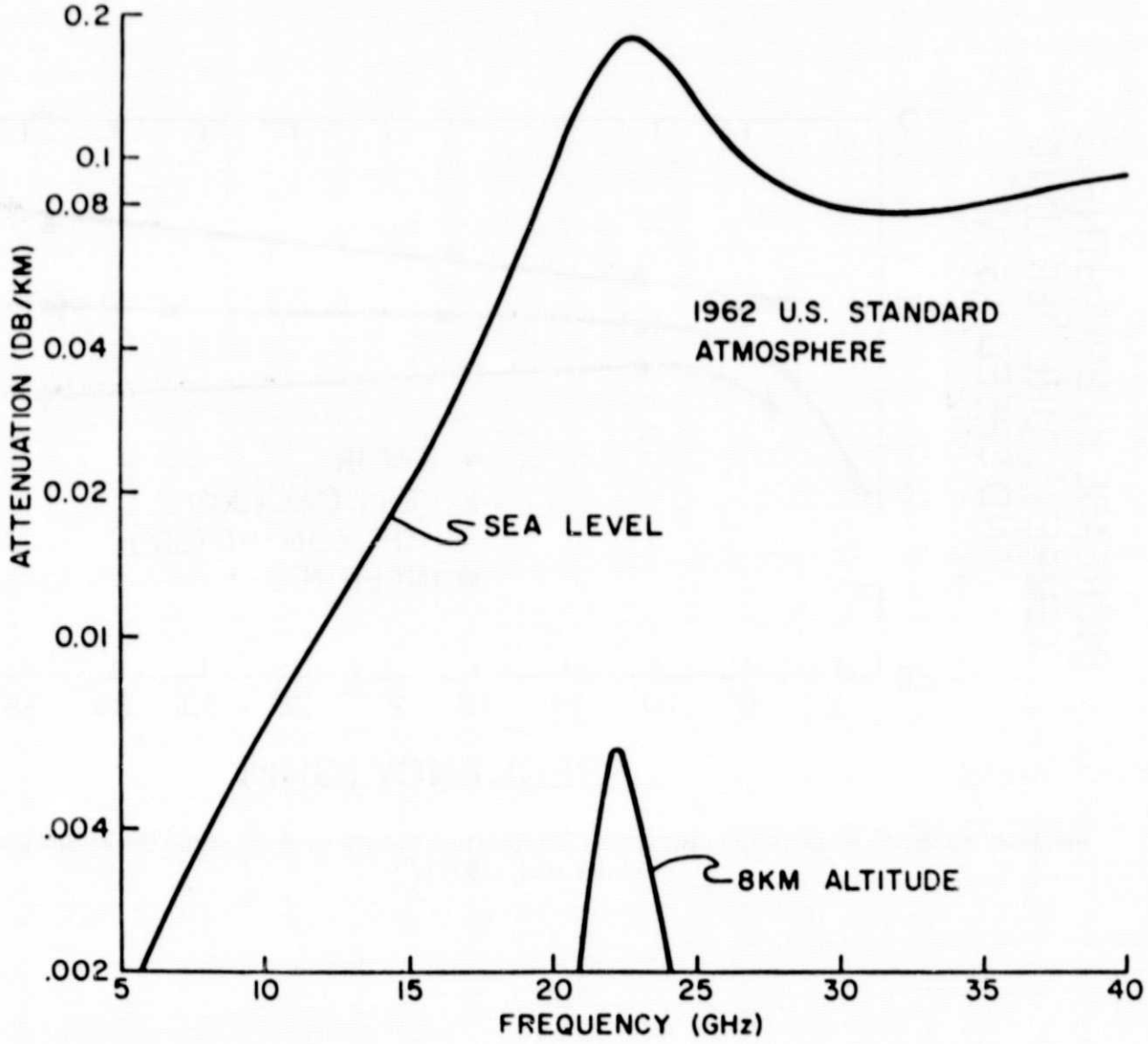

Figure 5. Microwave Absorption Coefficient for Atmospheric Water Vapor as a Function of Frequency

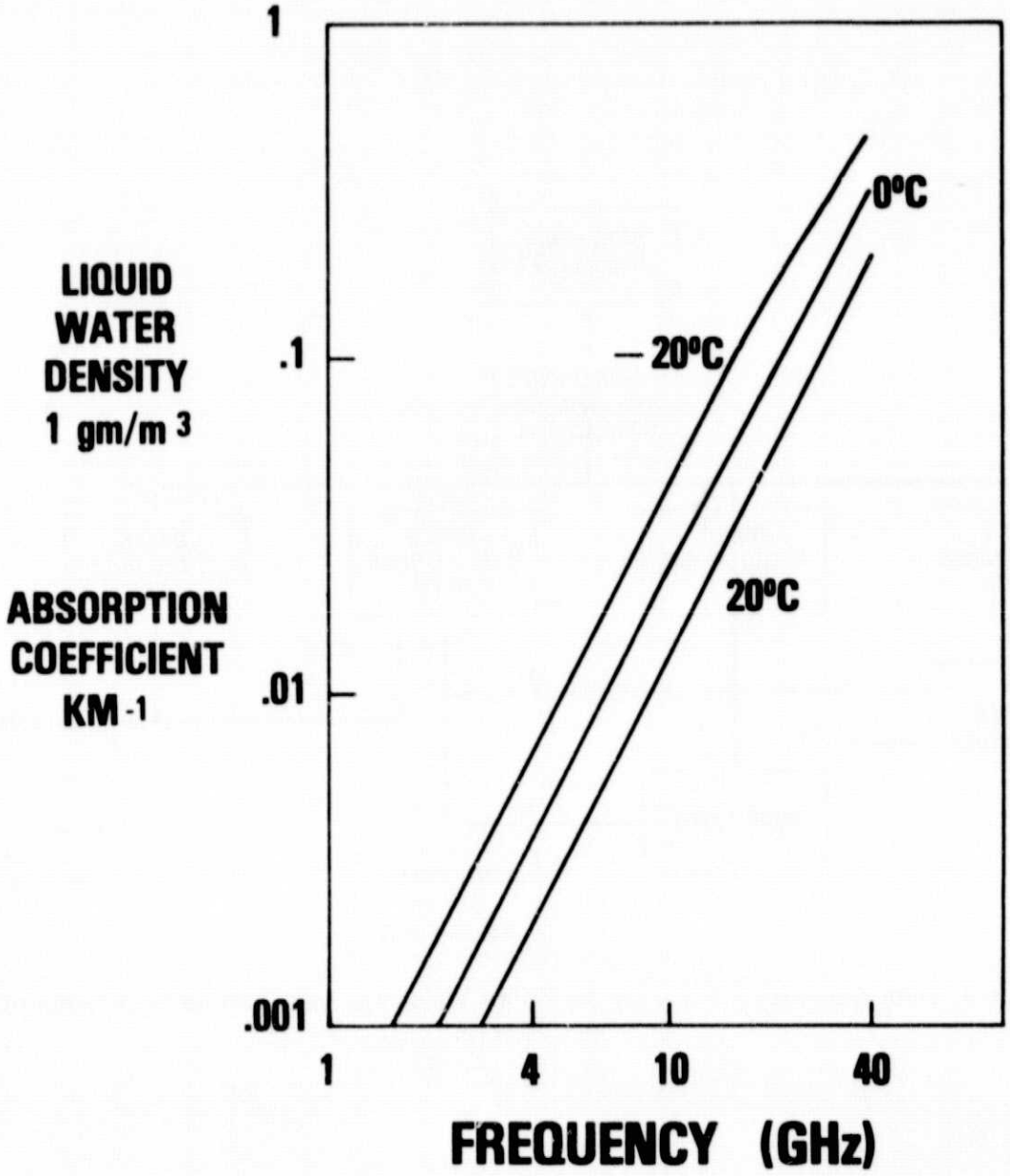

Figure 6. Microwave Absorption Coefficient for 1 gm/m^3 Concentration of Cloud Water Droplets

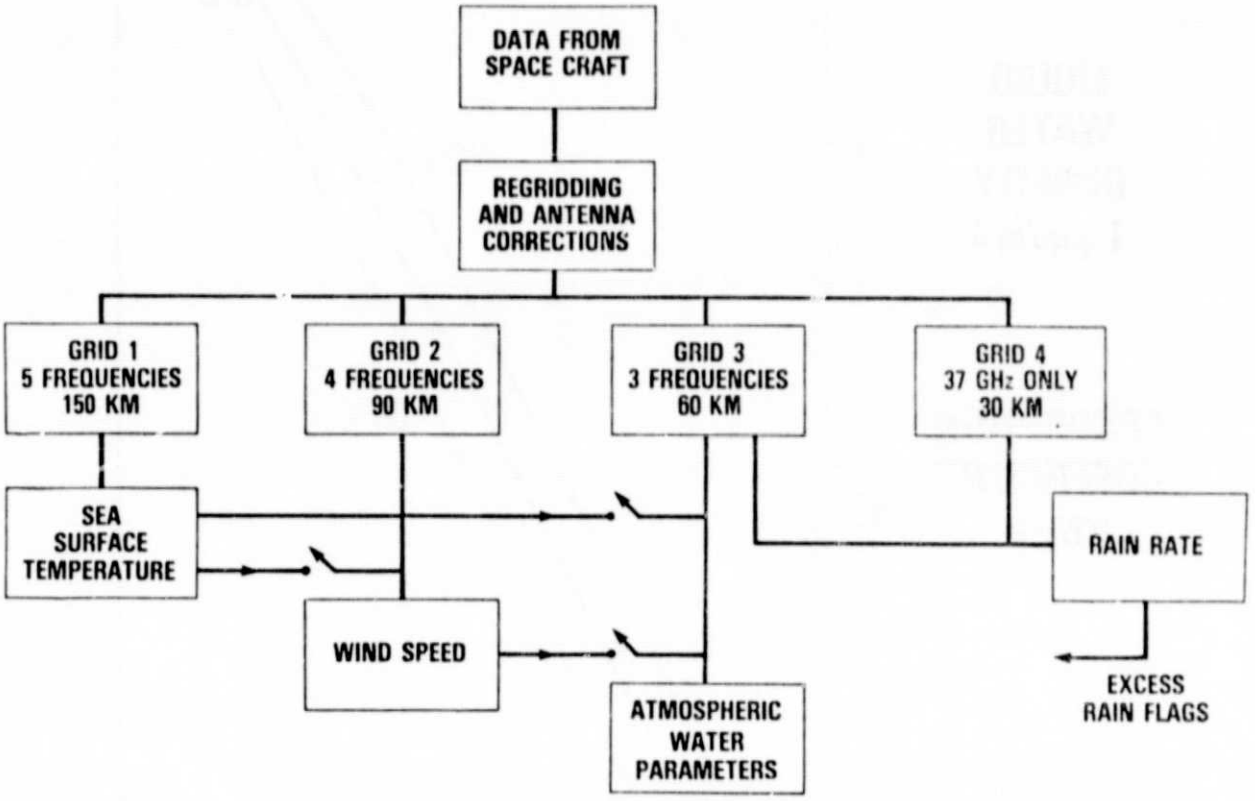

Figure 7. Data Processing Scheme for the SMMR Which was Launched on Both Nimbus-G and Seasat-A

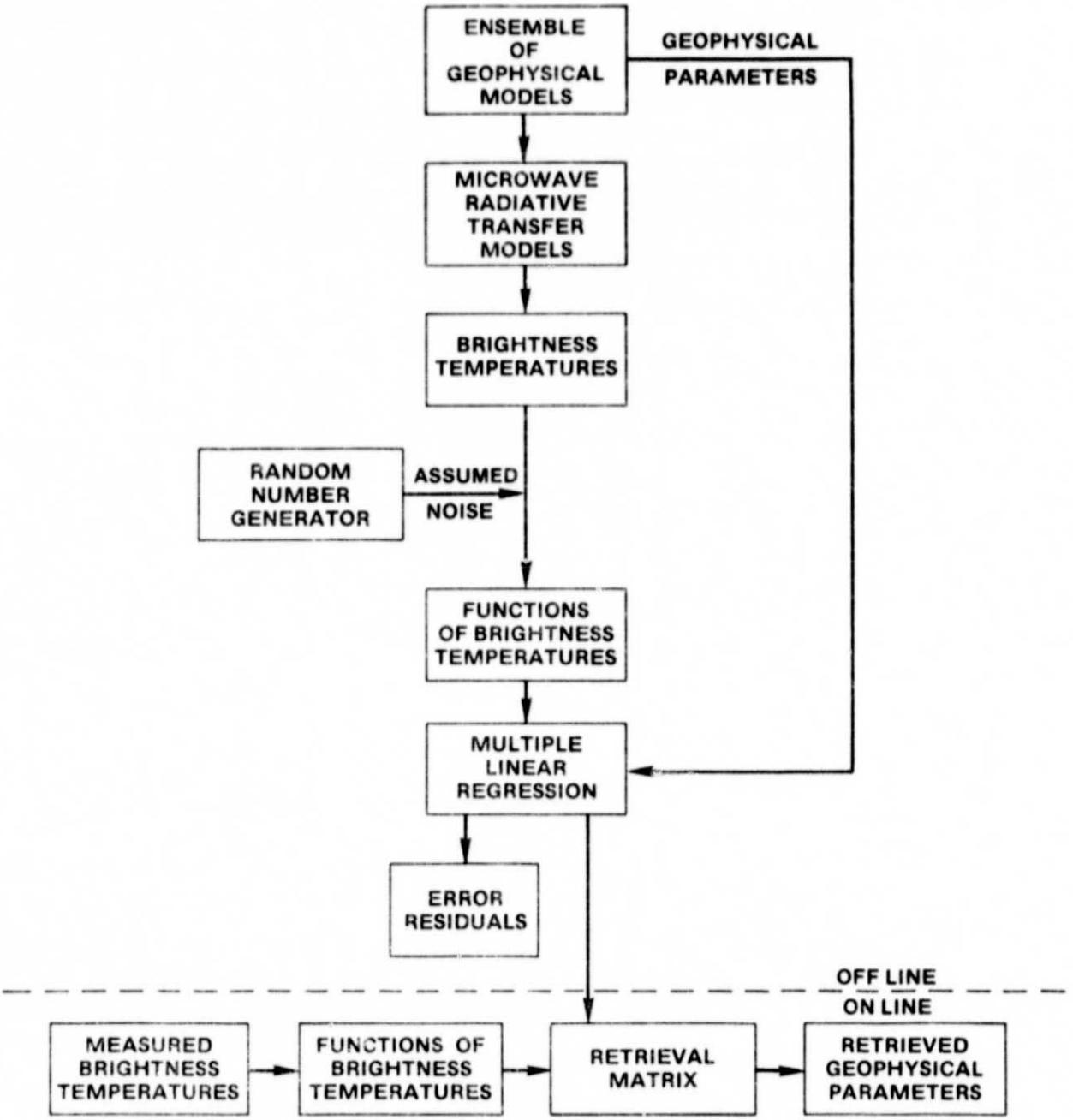

Figure 8. Logical Flow Diagram of Statistical Retrieval Technique